Multi-dimensional validation of a maximum-entropy-based interpolative moment closure

Boone R. Tensuda, James G. McDonald, and Clinton P. T. Groth

Citation: AIP Conference Proceedings **1786**, 140008 (2016); doi: 10.1063/1.4967639
View online: http://dx.doi.org/10.1063/1.4967639
View Table of Contents: http://scitation.aip.org/content/aip/proceeding/aipcp/1786?ver=pdfcov
Published by the AIP Publishing

Multi-Dimensional Validation of a Maximum-Entropy-Based Interpolative Moment Closure

Boone R. Tensuda[1], James G. McDonald[2] and Clinton P.T. Groth[1]

[1]*Institute for Aerospace Studies, University of Toronto, 4925 Dufferin Street, Toronto, Ontario, Canada*
[2]*Department of Mechanical Engineering, University of Ottawa, 161 Louis Pasteur, Ottawa, Ontario, Canada*

Abstract. The performance of a novel maximum-entropy-based 14-moment interpolative closure is examined for multi-dimensional flows via validation of the closure for several established benchmark problems. Despite its consideration of heat transfer, this 14-moment closure contains closed-form expressions for the closing fluxes, unlike the maximum-entropy models on which it is based. While still retaining singular behaviour in some regions of realizable moment space, the interpolative closure proves to have a large region of hyperbolicity while remaining computationally tractable. Furthermore, the singular nature has been shown to be advantageous for practical simulations. The multi-dimensional cases considered here include Couette flow, heat transfer between infinite parallel plates, subsonic flow past a circular cylinder, and lid-driven cavity flow. The 14-moment predictions are compared to analytical, DSMC, and experimental results as well the results of other closures. For each case, a range of Knudsen numbers are explored in order to assess the validity and accuracy of the closure in different regimes. For Couette flow and heat transfer between flat plates, it is shown that the closure predictions are consistent with the expected analytical solutions in all regimes. In the cases of flow past a circular cylinder and lid-driven cavity flow, the closure is found to give more accurate results than the related lower-order maximum-entropy Gaussian and maximum-entropy-based regularized Gaussian closures. The ability to predict important non-equilibrium phenomena, such as a counter-gradient heat flux, is also established.

INTRODUCTION AND MOTIVATION

Moment closure techniques [1, 2, 3, 4] are potentially both more robust and computationally lower-cost methods for simulating non-equilibrium transition-regime flows, relative to other approaches. These techniques provide approximate solutions to the Boltzmann equation in terms of solutions to a finite system of partial differential equations, which themselves represent transport of velocity moments of the particle phase-space distribution function. The system is closed by assuming a certain form of this distribution function. Since the method does not model particles directly and is of lower dimensionality compared to the Boltzmann equation, it has reduced computational cost relative to the discretized Boltzmann equation and direct-simulation Monte Carlo technique (DSMC) [5, 6].

A hierarchy of moment closures having a number of desirable properties has been derived based on the maximization of thermodynamic entropy [7, 8, 9]. Not only are these closures physically intuitive and mathematically elegant, but they have several practical advantages over traditional closures, such as those resulting from the Grad or Chapman-Enskog methods. The purely hyperbolic and first-order quasilinear nature of these moment closures presents numerical advantages which extend into both the transition and continuum regimes [1, 10]. These hyperbolic systems are less sensitive to grid irregularities, and only require evaluating first derivatives, which means that an extra order of spatial accuracy can often be gained using the same stencil. Furthermore, the maximum-entropy closures are not based on an expansion about the equilibrium distribution, and are therefore potentially more robust.

Unfortunately, complications encountered when considering closures of this type that contain a treatment for higher-order moments, such as heat transfer, have severely limited their use for general non-equilibrium flows. More specifically, the closing fluxes found based on the maximization of entropy cease to have a closed and continuous form. Nevertheless, a new, interpolative-type, maximum-entropy-based 14-moment closure has been proposed by McDonald and Torrilhon [11], based on previous ideas by McDonald and Groth [1], that successfully navigates the aforementioned problems. This closure has been applied to model internal shock structure, and it was found that it could do so without developing sub-shocks, even at high Mach numbers [11]. This study presents a further validation of this novel closure method for a range of multi-dimensional non-equilibrium flows.

30th International Symposium on Rarefied Gas Dynamics
AIP Conf. Proc. 1786, 140008-1–140008-8; doi: 10.1063/1.4967639
Published by AIP Publishing. 978-0-7354-1448-8/$30.00

Background

This section will review important concepts relevant to moment closures and introduce the notation used herein. The expected number of particles at a certain time, t, within an infinitesimal volume confined by, x_i to $x_i + \mathrm{d}^3 x_i$, and velocity v_i to $v_i + \mathrm{d}^3 v_i$, is $\mathcal{F}(x_i, v_i, t)\,\mathrm{d}^3 x_i\,\mathrm{d}^3 v_i$, where $\mathcal{F}(x_i, v_i, t)$ is the phase-space distribution function [2]. Common macroscopic engineering values can be computed from the phase-space distribution function by taking velocity moments. Some pertinent moments and their corresponding weightings are as follows:

$$\rho = \langle m\mathcal{F}\rangle, \quad u_i = \langle m v_i \mathcal{F}\rangle\,\rho, \quad p = \langle m c_i c_i \mathcal{F}/3\rangle, \quad q_i = \left\langle m c_i c_j c_j \mathcal{F}/2\right\rangle, \quad r = \left\langle m c_i c_i c_j c_j \mathcal{F}/15\right\rangle$$

$$P_{ij} = \langle m c_i c_j \mathcal{F}\rangle, \quad Q_{ijk} = \langle m c_i c_j c_k \mathcal{F}\rangle, \quad R_{ijkl} = \langle m c_i c_j c_k c_l \mathcal{F}\rangle, \quad S_{ijklm} = \langle m c_i c_j c_k c_l c_m \mathcal{F}\rangle,$$

where ρ is the density, u_i is the bulk velocity, $c_i = v_i - u_i$, is the random velocity, p is the hydrostatic pressure, P_{ij} is the anisotropic pressure tensor, Q_{ijk} is the heat-flux tensor, q_i is the heat-flux vector, R_{ijkl} and r are the fourth-order and contracted fourth-order moments, respectively, and S_{ijklm} is the fifth-order moment. The notation $\langle\cdot\rangle$ represents integration over all velocity space.

The evolution of the general phase-space distribution function in time and space is described by the Boltzmann equation. Moments of each term in the Boltzmann equation can be taken to obtain a transport equation for the corresponding macroscopic quantity. In general, a set of N transport equations can be found by defining a vector of N velocity weights, $\mathbf{W}^{(\mathbf{N})} = m[W_0, W_1, W_2, \ldots, W_N]^{\mathrm{T}}$. The resulting transport equations, known as Maxwell's equations of change, are

$$\frac{\partial}{\partial t}\langle \mathbf{W}^{(\mathbf{N})}\mathcal{F}\rangle + \frac{\partial}{\partial x_i}\langle v_i \mathbf{W}^{(\mathbf{N})}\mathcal{F}\rangle = \left\langle \mathbf{W}^{(\mathbf{N})}\frac{\delta\mathcal{F}}{\delta t}\right\rangle. \tag{1}$$

In this study the collision term, $\langle \mathbf{W}^{(\mathbf{N})}\delta\mathcal{F}/\delta t\rangle$, is modeled using the relaxation time approximations, Bhatnagar-Gross-Krook (BGK) and Ellipsoidal-Statistical (ES-BGK) [12]; unless otherwise stated the BGK simplification is used. It should be noted that the flux dyad, $\partial\langle v_i \mathbf{W}^{(\mathbf{N})}\mathcal{F}\rangle/\partial x_i$, always contains moments of one higher order than the solution vector, $\partial\langle \mathbf{W}^{(\mathbf{N})}\mathcal{F}\rangle/\partial t$, and thus the equation system is not closed. In order to close the system the phase-space distribution function must be restricted to an assumed form, which has the same number of degrees of freedom as there are moments in the solution vector.

Maximum-Entropy Closures

The maximum-entropy closure technique assumes a phase-space distribution function which maximizes thermodynamic entropy, and is therefore the most probable distribution, while remaining consistent with a given set of moments. To attain this distribution two constraints are considered, firstly, the distribution function must be consistent with the moments in the solution vector, referred to as $\mathbf{M}^{(N)}$, and secondly the distribution must maximize thermodynamic entropy. After considering a Lagrange multipliers optimization technique, the resulting form of the distribution function is $\mathcal{F} = \mathrm{e}^{\boldsymbol{\alpha}^{\mathrm{T}}\mathbf{W}^{(N)}}$ [8]. The values of the Lagrange multipliers or coefficients, $\boldsymbol{\alpha}$, are chosen such that the distribution function is consistent with the known moments. For higher-order closures, when $\mathbf{W}$ contains super-quadratic velocity weights, the moment integrals cannot be expressed in closed form. In this case, the coefficients must be found by solving the associated so-called maximum-entropy problem [8].

This problem requires an iterative numeric integration procedure to generate the distribution function and closing fluxes, and therefore significant numerical expense is added; this is often prohibitive. However, a new interpolation technique has been proposed to navigate these issues [1, 11], which will be discussed in the following section. Furthermore, regions in physically realizable moment space develop, including the equilibrium state, within which the maximum-entropy problem cannot be solved. In these regions the approximate distribution does not remain bounded [13], leading to a singularity in the closing flux. In practical implementations, this issue has been shown to be both computationally manageable and advantageous in terms of solution accuracy [11].

14-MOMENT INTERPOLATIVE CLOSURE

The velocity weighting vector used to generate the 14-moment closure is, $\mathbf{W} = m[1, v_i, v_i v_j, v_i v_j v_j, v_i v_i v_j v_j]$. This velocity weighting vector is substituted into Maxwell's equations of change (Equation 1), resulting in a set of 14-moment equations for a three-dimensional monatomic gas,

$$\frac{\partial \mathbf{U}}{\partial t} + \frac{\partial \mathbf{F}_k}{\partial x_k} = \mathbf{S}, \tag{2}$$

where $\mathbf{U}$ is the vector of conserved variables, $\mathbf{F}_k$ is the flux dyad, and $\mathbf{S}$ is the source vector resulting from inter-particle collisions, which is found using the ES-BGK operator. These vectors are

$$\mathbf{U} = \begin{pmatrix} \rho \\ \rho u_i \\ \rho u_i u_j + P_{ij} \\ \rho u_i u_j u_j + u_i P_{jj} + 2u_j P_{ij} + Q_{ijj} \\ \rho u_i u_i u_j u_j + 2u_i u_i P_{jj} + 4u_i u_j P_{ij} + 4u_i Q_{ijj} + R_{iijj} \end{pmatrix}, \tag{3}$$

$$\mathbf{F}_k = \begin{pmatrix} \rho u_k \\ \rho u_i u_k + P_{ik} \\ \rho u_i u_j u_k + u_i P_{jk} + u_j P_{ik} + u_k P_{ij} + Q_{ijk} \\ \rho u_i u_k u_j u_j + u_i u_k P_{jj} + 2u_i u_j P_{jk} + 2u_j u_k P_{ij} + u_j u_j P_{ik} + u_i Q_{kjj} + u_k Q_{ijj} + 2u_j Q_{ijk} + R_{ikjj} \\ \rho u_k u_i u_i u_j u_j + 2u_k u_i u_i P_{jj} + 4u_i u_i u_j P_{jk} + 4u_i u_j u_k P_{ij} + 2u_i u_i Q_{kjj} + 4u_i u_k Q_{ijj} + 4u_i u_j Q_{ijk} + 4u_i R_{ikjj} + u_k R_{iijj} + S_{kiijj} \end{pmatrix}, \tag{4}$$

$$\mathbf{S} = \begin{pmatrix} 0 \\ 0 \\ (3\tau)^{-1}(\delta_{ij} P_{kk} - 3P_{ij}) \\ (3\tau)^{-1}\left[2u_i(\delta_{ij} P_{kk} - 3P_{ij}) - 6u_i P_{jk} - 3\mathrm{Pr} Q_{ijj}\right] \\ (3\tau)^{-1}\left\{\frac{1}{\rho \mathrm{Pr}}[(3\mathrm{Pr}^2 + 4\mathrm{Pr} - 2)P_{ii}P_{jj} + 6(\mathrm{Pr} - 1)^2 P_{ij}^2] - 3\mathrm{Pr} R_{iijj} - 12\mathrm{Pr} u_i Q_{ijj} + 4u_i u_j \left(\delta_{ij} P_{kk} - 3P_{ij}\right)\right\} \end{pmatrix}, \tag{5}$$

where τ is a characteristic relaxation time scale and Pr is the Prandtl number. Setting Pr=1 recovers the BGK operator.

The moments, Q_{ijk}, R_{ijkk}, and S_{ijjkk} in the flux vector must be approximated to close the system. It has been shown that when considering super-quadratic velocity weightings, the maximum-entropy problem and associated closing flux ceases to have a closed-form solution, and a very expensive numerical procedure is required. In order to circumvent this problem, the interpolative closure of McDonald and Torrilhon [11] approximates the closing fluxes of the equivalent maximum-entropy using closed-form expressions. For convenience the realizable space is mapped to a new variable, σ. In the case of the 14-moment closure, σ is related to the known moments such that the following equality is satisfied,

$$R_{iijj} = \frac{1}{\sigma} Q_{kii} (P^{-1})_{kl} Q_{ljj} + \frac{2(1-\sigma) P_{ji} P_{ij} + P_{ii} P_{jj}}{\rho} \quad \sigma \in [0, 1]. \tag{6}$$

Expressions for the closing fluxes as a function of known moments, ρ, u_i, P_{ij}, Q_{ijj}, and R_{iijj}, can then be postulated using the interpolative method, which is fully described by McDonald and Torrilhon [11]. The resulting closing fluxes are

$$Q_{ijk} = \frac{P_{il}(P^2)_{jk} + P_{kl}(P^2)_{ij} + P_{jl}(P^2)_{ik}}{P_{lm}(P^2)_{\alpha\alpha} + 2(P^3)_{lm}} Q_{mnn}, \quad R_{ijkk} = \frac{1}{\sigma} Q_{ijl} (P^{-1})_{lm} Q_{mkk} + \frac{2(1-\sigma) P_{ik} P_{kj} + P_{ij} P_{kk}}{\rho}, \tag{7}$$

$$S_{ijjkk} = \frac{Q_{npp} Q_{mjj} Q_{ikl}}{\sigma^2 P_{kn} P_{lm}} + 2\sigma^{\frac{1}{2}} \frac{P_{jj} Q_{ikk}}{\rho} + (1 - \sigma^{\frac{1}{2}}) W_{ij} Q_{mnn}, \tag{8}$$

where

$$W_{ij} = \frac{P_{il}(P_{\alpha\alpha})^3 + 6P_{il}(P^3)_{\alpha\alpha} + 7(P^2)_{\alpha\alpha}(P^2)_{il} + 10P_{\alpha\alpha}(P^3)_{il} + 10(P^4)_{il} - (P^2)_{\alpha\alpha} P_{\beta\beta} O_{il} - 3(P_{\alpha\alpha})^2 (P^2)_{il}}{\rho P_{lm}(P^2)_{\alpha\alpha} + 2(P^3)_{lm}}. \tag{9}$$

The 14-moment equation system presented above is solved on multi-block quadrilateral grids in two-dimensions using a second-order, Godunov-type, finite-volume scheme. Both a semi-implicit and fully-implicit (via a Newton-Krylov-Schwarz (NKS) method) time marching technique were used [14, 15]. For this preliminary study, solid-wall boundary conditions based on standard Knudsen-layer analysis [10] are used. Although a full analysis of the proposed approximate boundary conditions and resulting Knudsen layers, similar to that considered in [16] for a regularized 13-moment system, has not been conducted, the procedure proved adequate for obtaining the first multi-dimensional solutions of the 14-moment closure presented here and future follow-on studies will explore the question of boundary condition in more detail. The technique requires that the internal phase-space distribution be known; however, for the 14-moment interpolative closure, analytical expressions for the internal distribution in terms of the known moments are not available. To avoid a numerical treatment and arrive at analytical expressions for the boundary conditions of the closure, in this study a Grad-like perturbative expansion applied to the Gaussian distribution function (the 10-moment maximum-entropy solution) has been used as the interior distribution [17]. The resulting expressions, where the solid-wall is oriented with a normal in the negative x-direction towards the interior of the fluid domain, are:

$$n_{\mathrm{Kn}} = \frac{(2-\mathcal{A})}{2\sqrt{\pi}P_{xx}^{3/2}m}\left\{\sqrt{\pi}\rho P_{xx}^{3/2} - \frac{\sqrt{2}}{5}D_x\sqrt{\rho}\left(P_{xy}^2 + P_{xx}^2\right)\right\} + \frac{\mathcal{A}n_w}{2}, \qquad u_{x\mathrm{Kn}} = 0, \tag{10}$$

$$u_{y\mathrm{Kn}} = \frac{-3(2-\mathcal{A})\,n}{2\sqrt{\pi}P_{xx}^{5/2}\rho^3 n_{\mathrm{Kn}}}\left\{\frac{\sqrt{2}}{15}\rho^{5/2}P_{xx}\left(D_xP_{xx}^2u_y - 5P_{xx}P_{xy} + D_xP_{xy}^2u_y\right) - \frac{\sqrt{\pi}}{3}\rho^3P_{xx}^{5/2}u_y + \sqrt{2}E\sqrt{\rho}P_{xy}\left(P_{xx}^2 + P_{xy}^2\right)\left(P_{xx}^2 + 4P_{xx}P_{yy} - 3P_{xy}^2\right)\right\} + \frac{\mathcal{A}n_w}{2n_{\mathrm{Kn}}}u_{wy}, \tag{11}$$

$$P_{xy\mathrm{Kn}} = \frac{(2-\mathcal{A})}{2\sqrt{\pi}\rho^2P_{xx}^{3/2}}\left\{\frac{\sqrt{2}}{5}\rho^{3/2}\left[D_yP_{xx}^3 + D_xP_{xx}^2P_{xy} + P_{xx}P_{xy}\left(D_yP_{xy} + 2D_xP_{yy}\right) - D_xP_{xy}^3\right] - \sqrt{2}\rho^{5/2}P_{xx}^2\left(u_{y\mathrm{Kn}} - u_y\right) + \sqrt{\pi}\rho^2P_{xx}^{3/2}P_{xy} + 3\sqrt{2}E\sqrt{\rho}\left(P_{xx}^2 + P_{xy}^2\right)^2\left(u_{y\mathrm{Kn}} - u_y\right)\right\} - \mathcal{A}\sqrt{\frac{n_w\rho_wkT_w}{2\pi}}\left(u_{wy} - u_{y\mathrm{Kn}}\right), \tag{12}$$

$$\begin{aligned} Q_{xii\mathrm{Kn}} = {} & \frac{9(2-\mathcal{A})\rho}{2\sqrt{\pi}\rho^4P_{xx}^{5/2}}\left\{\frac{2\sqrt{\pi}}{15}D_x\rho^2P_{xx}^{9/2} - \frac{1}{3}P_{xx}^5(P_{yy}+P_{zz}) + \frac{8\sqrt{\pi}}{45}\rho^2P_{xx}^{5/2}\left[\frac{1}{4}D_x(P_{yy}^2+P_{zz}^2) + P_{xy}\left(-\frac{5}{4}\rho u_{y\mathrm{Kn}} + \frac{5}{4}\rho u_y + \frac{1}{2}D_yP_{yy}\right) + D_xP_{xy}^2\right] + \frac{4\sqrt{\pi}}{45}D_y\rho^2P_{xx}^{7/2}P_{xy}\right. \\ & + \frac{\sqrt{2}}{9}\rho^{7/2}P_{xx}^3(u_{y\mathrm{Kn}}-u_y)^2 - \frac{\sqrt{2}}{3}E\rho^{3/2}P_{xx}(P_{xx}^2+P_{xy}^2)^2(u_{y\mathrm{Kn}}-u_y)^2 + \frac{2\sqrt{2}}{45}\rho^{5/2}P_{xx}\left[-P_{xx}P_{xy}\left(P_{xy}\left(D_yu_{y\mathrm{Kn}} - D_yu_y - \frac{5}{2}\right) + 2D_xP_{yy}(u_{y\mathrm{Kn}}-u_y)\right)\right. \\ & + P_{xx}^2\left(-D_xP_{xy}\left(u_{y\mathrm{Kn}}-u_y\right) + \frac{5}{2}P_{yy} + \frac{5}{2}P_{zz}\right) + P_{xy}^3D_x(u_{y\mathrm{Kn}}-u_y) + P_{xx}^3\left(5 + D_y(u_y - u_{y\mathrm{Kn}})\right)\Big] + \sqrt{2}\sqrt{\rho}E\Big[2P_{xx}^6 + P_{xy}^6 + \frac{1}{3}P_{xx}^4(19P_{xy}^2 + 4P_{yy}^2 + 4P_{zz}^2) \\ & \left.\left. + \frac{8}{3}P_{xx}^2P_{xy}^2\left(\frac{1}{2}P_{zz}^2 + \frac{3}{2}P_{yy}^2 + P_{xy}^2\right) + 2P_{xx}^3P_{xy}^2\left(P_{yy} - \frac{1}{3}P_{zz}\right) - 3P_{xx}P_{xy}^4(P_{yy} + \frac{1}{9}P_{zz})\Big]\right\} - \frac{\mathcal{A}\rho_w\sqrt{kT_w}}{\sqrt{2\pi}m^{3/2}}\left[m(u_{y\mathrm{Kn}}-u_{yw})^2 + 4kT_w\right], \end{aligned} \tag{13}$$

where the values of D_i and E are determined through the relations,

$$q_i = \frac{1}{5\rho}\left[P_{jk}^2D_i + 2P_{ik}P_{jk}D_j\right], \quad \text{and} \quad E = \frac{5\rho^3}{8}\frac{r - \left(P_{ii}P_{jj} + 2P_{ij}^2\right)/15\rho}{\left[P_{ik}^2P_{jl}^2 + 2P_{ik}P_{il}P_{jk}P_{jl}\right]}, \tag{14}$$

where $\mathcal{A}$ is the accommodation coefficient, and u_{wy} and T_w are the wall velocity and temperature, respectively. An interesting result of the formulated boundary conditions is the coupling between the shear stress, P_{xy}, and heat flux, Q_{xii} and Q_{yii}. The fully-implicit NKS solver helps to manage the resulting large non-linearity, particularly in the transition regime.

RESULTS AND DISCUSSION

Couette Flow and Heat Transfer

The Couette flow case which has been studied consists of two parallel, fully-accommodating, plates moving in opposite directions at a velocity, U_w, of 30 m s^{-1} in the x-direction. The gas between the plates is argon with standard atmospheric free stream density of 1.225 kgm^{-3} and pressure of 101.325 kPa, and therefore a temperature of 397.37 K. The temperature of the plates, T_w, is 397.37 K to ensure minimal heat transfer between the plates and internal gas. The results for the normalized flow velocity, u_x/U_w, and shear stress, normalized with respect to the free-molecular value, for a wide range of Knudsen numbers are shown in Figure 1. These computed values are compared with results found using the Gaussian closure [1], a 10-moment maximum-entropy closure, and an analytical solution developed by Lees [18]. It is evident that the predicted values of the 14-moment closure are in very good agreement with those of the Gaussian closure and Lees solution throughout the continuum, transition, and free-molecular regimes.

In the case of heat transfer between infinite flat plates the plates are stationary and the upper and lower plate temperatures have been set to 407.37 K and 387.37 K, respectively; resulting in a temperature difference of 20 K between the plates. The results are presented in Figure 2, including a comparison of the BGK and ES-BGK collision operators. The wall temperature has been normalized as, $T^* = (T - T_m)/(T_w - T_m)$, where T is the temperature of the gas adjacent to the wall and T_m is the gas temperature midway between the plates. The heat flux between the plates has been normalized with respect to the free-molecular heat flux [19]. The results are compared to the free-molecular solution, the continuum NSF solution, and the NSF solution with temperature jump boundary conditions [19]. Overall the results from the 14-moment interpolative closure with the ES-BGK collision operator are in very good agreement with the analytic NSF solution with slip boundary conditions, and agree with the continuum and free-molecular solutions at low and high Knudsen numbers, respectively.

Subsonic Flow Past a Circular Cylinder

Subsonic flow past a circular cylinder is considered for several Knudsen numbers spanning the transition regime and two speed ratios, S, of 0.027 and 0.107. For comparison, simulations were also carried out using the Gaussian

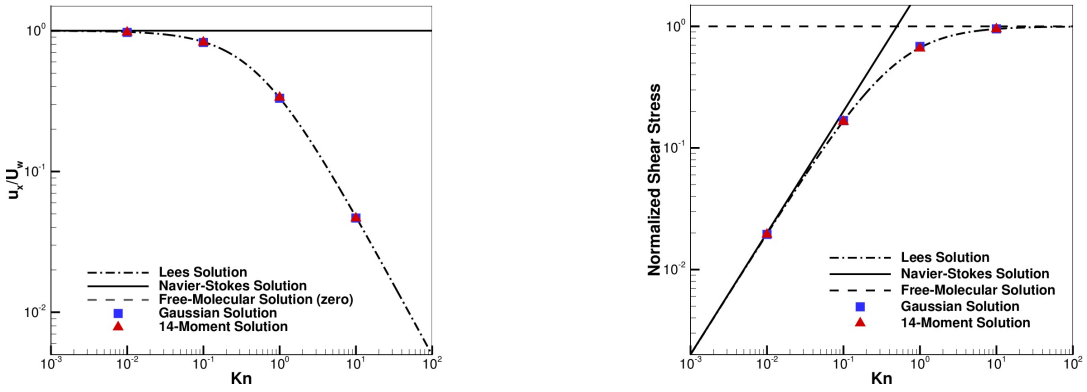

FIGURE 1: *Normalized flow velocity at the plate as a function of Knudsen number (left). Normalized shear stress between the plates with respect to Knudsen number (right).*

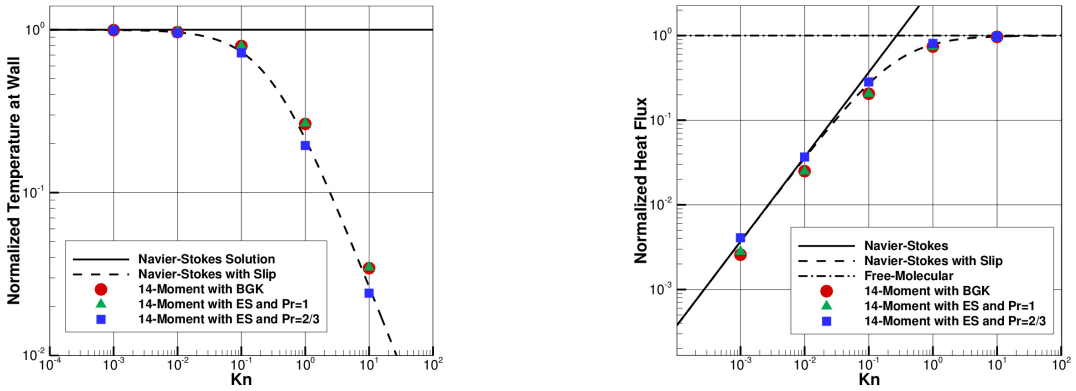

FIGURE 2: *Results for heat transfer between infinite flat plates showing normalized temperature at the wall (left) and heat flux between the plates as a function of Knudsen number (right). The improvements in accuracy from the ES-BGK model relative to the BGK model are clear.*

closure [1, 14] and the regularized Gaussian closure [1, 20], which is a 10-moment maximum-entropy closure with added approximations for heat flux. In Figure 3 (a), the predicted values of the drag coefficient, c_d, are compared with experimental values found by Coudeville *et al.* [21]. Although these experimental values were found for air, they are expected to be very similar to those of argon due to their similar viscosity. The values of drag coefficient predicted by the 14-moment closure are in excellent agreement with those of the Gaussian closure and experiment for the lower Knudsen number cases of Kn=0.01 and Kn=0.1. This was anticipated since the contributions of heat transfer are small. As the free-molecular regime is approached the predicted drag coefficients for the closure methods begin to diverge. However, the 14-moment closure seems to follow the trends of the experimental results more closely than the Gaussian closure. This is expected since the 14-moment closure considers a higher number of moments, and thus should remain valid to a higher Knudsen number. These results are promising as they not only validate the 14-moment closure at low Knudsen numbers, but also show its improved predictive capabilities at higher Knudsen numbers. Aside from an improvement in drag prediction, the 14-moment closure was also able to predict the non-equilibrium phenomena of temperature polarization and counter-gradient heat flux. This effect can be seen in Figure 3 (c) where the temperature contours and heat-flux streamlines around the cylinder at Kn=1 are shown. It is observed that the heat flux is oriented in the opposite direction to that expected based on Fourier's law. This effect has been previously observed when considering flows in the transition regime, such as in analytical solutions for flow around a sphere by Torrilhon [22]. The 14-moment closure's ability to predict this phenomenon is very promising, as it is not predicted by lower-order maximum-entropy closures such as the 10-moment Gaussian closure or maximum-entropy-based closures such as the regularized Gaussian closure (see Figure 3 (b)).

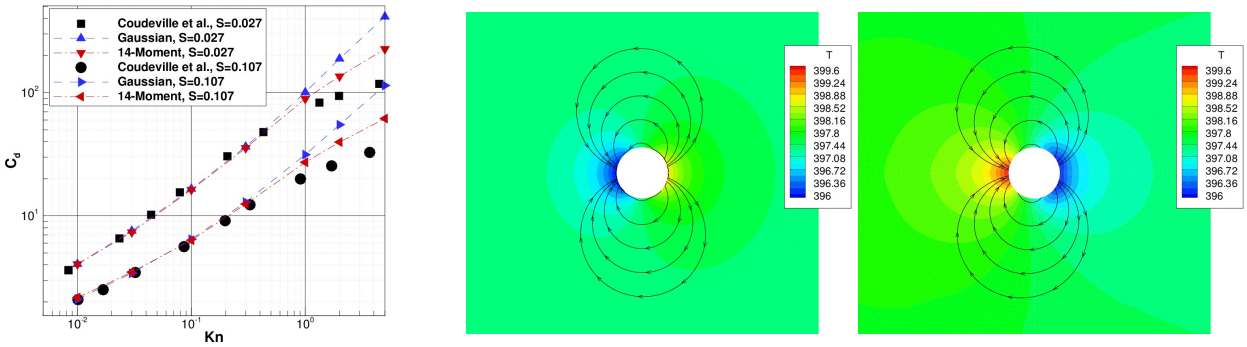

(a) (b) (c)

FIGURE 3: *(a) Comparison of predicted drag coefficients found using the 14-moment and Gaussian closures and experimental values for air [21]. Temperature contours and heat-flux streamlines for subsonic flow past a circular cylinder at Kn=1 found by solving the (b) regularized Gaussian and (c) 14-moment closures.*

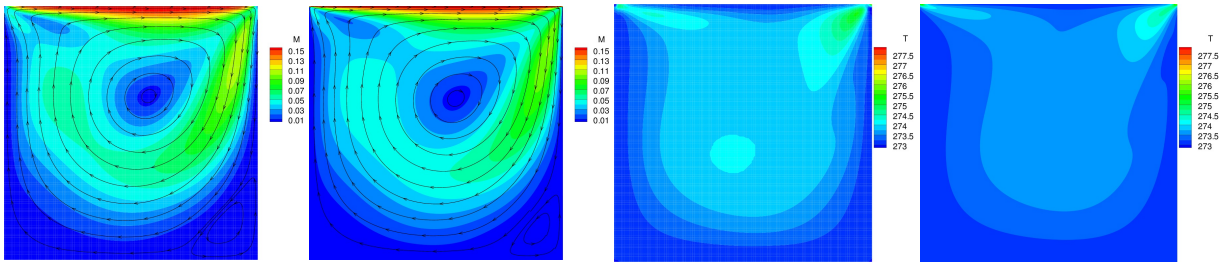

(a) (b) (c) (d)

FIGURE 4: *Mach number contours and velocity streamlines for the (a) 14-moment and (b) NSF solutions, and temperature contours and heat-flux streamlines for the (c) 14-moment and (d) NSF solutions of the lid-driven cavity at Kn=0.001.*

Lid-Driven Cavity Flow

Finally, the case of lid-driven cavity flow, with a lid velocity of $U = 50$ m s^{-1}, is considered. The square cavity contains argon with a temperature of 273 K. The wall temperatures are set equivalent to the initial gas temperature. Solutions are found in the continuum, Kn=0.001, and transition, Kn=0.1, regimes. These solutions are compared to results found using the NSF equations, for the continuum regime case, and the regularized Gaussian closure and a DSMC solution found by John, Gu, and Emerson [23], for the transition regime case. Note that the computational cost of solving moment equations is on the same order of magnitude as the NSF equations (the computational costs of the 14-moment closure is estimated to be only about 2-4 time more than that of the usual NSF model) and at least 2-3 orders of magnitude less expensive than the more mature DSMC methods [24], particularly for low-Mach-number and transition-regime flows. In the DSMC study, a variable hard sphere collision model is used. This may lead to some discrepancies with the 14-moment results, for which the BGK collision model is used. The resulting Mach number and temperature profiles for the Kn=0.001 case can be seen in Figure 4. The Mach number contours and velocity stream lines show good agreement, as expected. The temperature profiles are also in fair agreement for both solution techniques, showing an overall uniform temperature distribution, as expected in this regime.

Figure 5 displays the results of the transition regime, Kn=0.1, case for the regularized Gaussian closure, 14-moment closure, and DSMC results. Since heat flux is no longer negligible at this Knudsen number, the heat-flux streamlines are now overlaid on the temperature contours. Furthermore, the shear stress now becomes significant, and is plotted as well. The Mach number contours all display velocity slip at the lid as anticipated, however the slip seems to be slightly over-predicted in the regularized Gaussian solution, and thus the 14-moment solution is in better agreement with the DSMC results. The 14-moment solution's shear stress predictions are also in better agreement with the DSMC results. However, there is an over-prediction of shear stress adjacent to the lid surface. This is likely

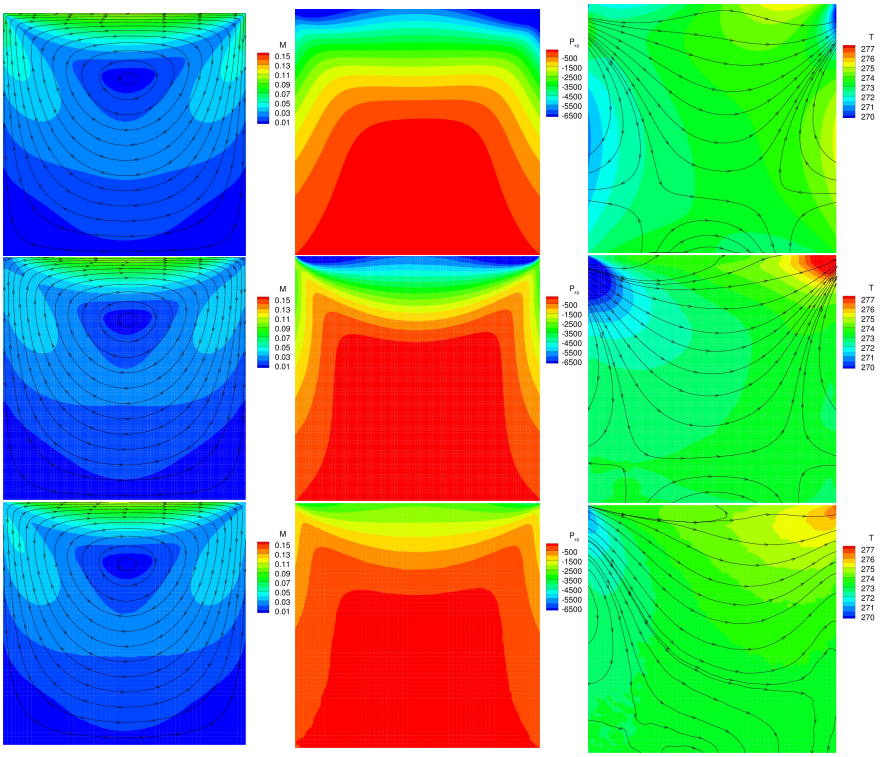

FIGURE 5: *(a) Mach number contours and velocity streamlines, (b) shear stress contours, and (c) temperature contours and heat-flux streamlines for the regularized Gaussian closure (top), 14-moment closure (middle) and DSMC solutions (bottom) of the lid-driven cavity at Kn=0.1 [23, 25].*

a result of deficiencies in the boundary condition, as opposed to the closure system itself.

Both the 14-moment closure and DSMC method predict a high-temperature region in the top right corner, and a low-temperature region in the top left corner, however the absolute temperature values are much larger for the 14-moment results. This low-temperature region is a consequence of gas cooling by expansion and the high-temperature region results from viscous dissipation [23, 25]. The regularized Gaussian closure predicts both high-temperature and low-temperature areas in each corner, which is inconsistent with the DSMC results. Interestingly, both the 14-moment closure technique and DSMC method predict a counter-gradient heat flux, similar to that seen in the cylinder case (Figure 3 (c)). It is noteworthy that despite the inclusion of heat transfer in the regularized Gaussian closure, it cannot reproduce the counter-gradient heat flux (see Figure 5 (c)), whereas a regularized version of the 13-moment Grad equations has been shown to reproduce these expected effects by Rana *et al.* [24]. The results of Figure 5 provide further demonstration of the relative importance and complexity of heat-transfer phenomena in non-equilibrium transport.

CONCLUSION

A new, 14-moment, maximum-entropy-based, interpolative closure has been investigated and employed to solve a variety of canonical two-dimensional flow problems. Solutions were obtained for Couette flow, heat transfer between infinite flat plates, subsonic flow past a circular cylinder and lid-driven cavity flow. The Couette flow and heat transfer cases had excellent agreement with analytic solutions, and in the latter case the ES-BGK collision operator was found to significantly increase accuracy. The circular cylinder results showed a drag prediction for low Knudsen numbers which is consistent with the experimental values and Gaussian closure, as well as an improved prediction of drag for high-Knudsen-number flows. The phenomena of counter-gradient heat flux was also observed. The 14-moment results

for the continuum lid-driven cavity flow were in good agreement with the NSF solution. Furthermore, the 14-moment closure was successful in predicting the presence of expansion cooling and viscous heating, as well as a counter-gradient heat flux, in the transition regime, which was also observed in a DSMC solution. Overall this study, one of the first for the maximum-entropy-based 14-moment interpolative closure for multi-dimensional flows, has demonstrated the closures promise due to: 1) its improved predictive capabilities and ability to predict non-equilibrium phenomena, such as counter-gradient heat flux, as compared to other similar closures; and 2) its significantly lower computational costs compared with DSMC and direct discretization methods applied to the Boltzmann equation.

ACKNOWLEDGMENTS

Computational resources were provided by the SciNet High Performance Computing Consortium at the University of Toronto and Computer/Calcul Canada through funding from the Canada Foundation for Innovation (CFI) and the Province of Ontario, Canada. The first author acknowledges the Province of Ontario for their support through an Ontario Graduate Scholarship. The authors also thank David R. Emerson, Benzi John, and Xiao-Jun Gu at STFC Daresbury Laboratory for providing the DSMC solutions for the the lid-driven cavity flow.

REFERENCES

[1] C. P. T. Groth and J. G. McDonald, Continuum Mech. Thermodyn. **21**, 467–493 (2009).
[2] T. I. Gombosi, *Gaskinetic Theory* (Cambridge University Press, Cambridge, 1994).
[3] H. Struchtrup, *Macroscopic Transport Equations for Rarefied Gas Flows* (Springer-Verlag, Berlin, 2005).
[4] M. Torrilhon, Ann. Rev. Fluid Mech. **48**, 429–458 (2016).
[5] L. Mieussens, Math. Mod. Meth. Appl. S. **10**, 1121–1149 (2000).
[6] G. A. Bird, *Molecular Gas Dynamics and the Direct Simulation of Gas Flows* (Clarendon Press, Oxford, 1994).
[7] W. Dreyer, J. Phys. A: Math. Gen. **20**, 6505–6517 (1987).
[8] C. D. Levermore, J. Stat. Phys. **83**, 1021–1065 (1996).
[9] I. Müller and T. Ruggeri, *Rational Extended Thermodynamics* (Springer-Verlag, New York, 1998).
[10] J. G. McDonald, J. S. Sachdev, and C. P. T. Groth, AIAA J. **52**, 1839–1857 (2014).
[11] J. G. McDonald and M. Torrilhon, J. Comput. Phys. **251**, 500–523 (2013).
[12] L. H. Holway, Jr., Phys. Fluids **9**, 1658–1673 (1966).
[13] M. Junk, J. Stat. Phys. **93**, 1143–1167 (1998).
[14] J. G. McDonald and C. P. T. Groth, "Numerical modeling of micron-scale flows using the Gaussian moment closure," Paper 2005-5035 (AIAA, 2005).
[15] Y. Saad, *Iterative Methods for Sparse Linear Systems* (PWS Publishing Company, Boston, 1996).
[16] H. Struchtrup and T. Thatcher, Continuum Mech. Thermodyn. **19**, 177–189 (2007).
[17] C. P. T. Groth, P. L. Roe, T. I. Gombosi, and S. L. Brown, "On the nonstationary wave structure of a 35-moment closure for rarefied gas dynamics," Paper 95-2312 (AIAA, 1995).
[18] W. G. Vincenti and C. H. Kruger, *Introduction to Physical Gas Dynamics* (R. E. Krieger Publishing, Huntington, NY, 1975).
[19] E. H. Kennard, *Kinetic Theory of Gases* (McGraw-Hill, New York, 1938).
[20] J. G. McDonald and C. P. T. Groth, "Extended fluid-dynamic model for micron-scale flows based on Gaussian moment closure," Paper 2008-0691 (AIAA, 2008).
[21] H. Coudeville, P. Trepaud, and E. A. Brun, "Drag measurements in slip and transition flow," in *Rarefied Gas Dynamics*, Vol. I, edited by J. H. de Leeuw (Academic Press, New York, 1965), pp. 444–466.
[22] M. Torrilhon, Phys. Fluids **22**, 1–16 (2010).
[23] B. John, X. J. Gu, and D. R. Emerson, Numer. Heat Trans. B **52**, 287–303 (2010).
[24] A. Rana, M. Torrilhon, and H. Struchtrup, J. Comput. Phys. **236**, 169–186 (2013).
[25] B. John, X. J. Gu, and D. R. Emerson, Computer & Fluids **45**, 197–201 (2011).